Elastic anisotropic finite-difference full-wave modeling and imaging of the tilted transversely isotropic (TTI) media

Laxmidhar Behera, CSIR-National Geophysical Research Institute, India*
**E-mail: laxmidhar@ngri.res.in*

Keywords
Anisotropy; VTI; TTI; Staggered grid; Modeling; Synthetic seismic data

Summary

Imaging below the tilted transversely isotropic (TTI) media poses serious problems and distortions in the image, which is very common with imaging subsurface geological targets for hydrocarbon exploration in the fold-thrust belts or active tectonic areas. To model and image below the TTI media having symmetry axis orthogonal to the dipping anisotropic layers, a TTI thrust sheet is considered for elastic anisotropic finite-difference full-wave modeling to generate synthetic seismic data using staggered grid scheme of wave propagation. Free surface conditions at the top and absorbing boundary conditions for other three sides of the model have been imposed to reduce undesirable edge effects and suppress dispersions. The synthetic data generated are migrated using the Kirchhoff pre-stack depth migration (PSDM) technique followed by migration velocity analysis (MVA) algorithm with traveltime computations using anisotropic ray-tracing technique for the model to image below the TTI thrust sheet. The MVA algorithm adopted also estimates the final inversion parameters of the model showing flattening of the reflected events in the image gathers and is a powerful tool to handle tilts more than 60° without much distortions of the image gathers.

Introduction

The subsurface geological structures are generally heterogeneous and anisotropic. Modeling with the help of algorithms based on homogeneous and isotropic approximations leads to inaccurate positioning of target zones within the earth as well as cause serious limitations of imaging. Transverse isotropy (TI) is considered as one of the most common anisotropic models prevalent within the subsurface earth and mainly associated with sedimentary formations having periodic fine layering such as shales. Horizontally layered sediments are characterized by TI media with a vertical symmetry axis (VTI) and may be horizontal transversely isotropic (HTI) if the host rock has only vertical fracture zones. However, in active tectonic areas, the anisotropic layers may be dipping, which leads to a TI media with tilted axis of symmetry (TTI). The TTI models are typical examples of up-tilted shale layers near salt domes with a large inclination of the symmetry axis (Behera and Tsvankin, 2009) and in over-thrust areas such as Canadian Foothills or Himalayan Foothills, where TI shale layers are often bent by tectonic processes due to which the dips of the layers generally exceeds 45° (Grechka *et al*., 2001).

The presence of TTI formations in over-thrust areas may cause severe problems in imaging of target zones for exploration of hydrocarbon. Ignoring the influence of anisotropy and by simply applying conventional (isotropic) velocity-analysis and migration techniques definitely leads to mispositioning and poor focusing of target reflectors beneath the TTI layers (Isaac and Lawton, 1999; Vestrum et al., 1999; Grechka *et al*., 2001; Behera and Tsvankin, 2009). A TTI layer is generally characterized by five Thomsen's (1986) parameters i.e., V_{P0} (*P*-wave velocity in the symmetry direction), V_{S0} (*S*-wave velocity in the symmetry direction), ϵ (a measure of *P*-wave anisotropy), δ (parameter controlling near vertical wave propagation) and γ (a measure of *S*-wave anisotropy) along with variable tilts (ν) corresponding to each anisotropic blocks. *P*- and *SV*-wave propagations in the plane containing the symmetry axis do not depend on parameter γ, and hence the wave propagation is characterized by four parameters V_{P0}, V_{S0}, ϵ and δ (Thomsen, 1986). Further simplification for *P*-wave propagation follows from the assumption of 'weak' anisotropy where the effect of V_{S0} on *P*-waves is negligible (Thomsen, 1986). Hence *P*-wave propagation in the TTI thrust sheet can be characterized fully by three Thomsen's parameters as V_{P0}, ϵ, δ and the thickness (Kumar *et al*., 2008). The TTI thrust sheet resembles

NGRI, Uppal Road, Hyderabad-500007, India, email: laxmidhar@ngri.res.in

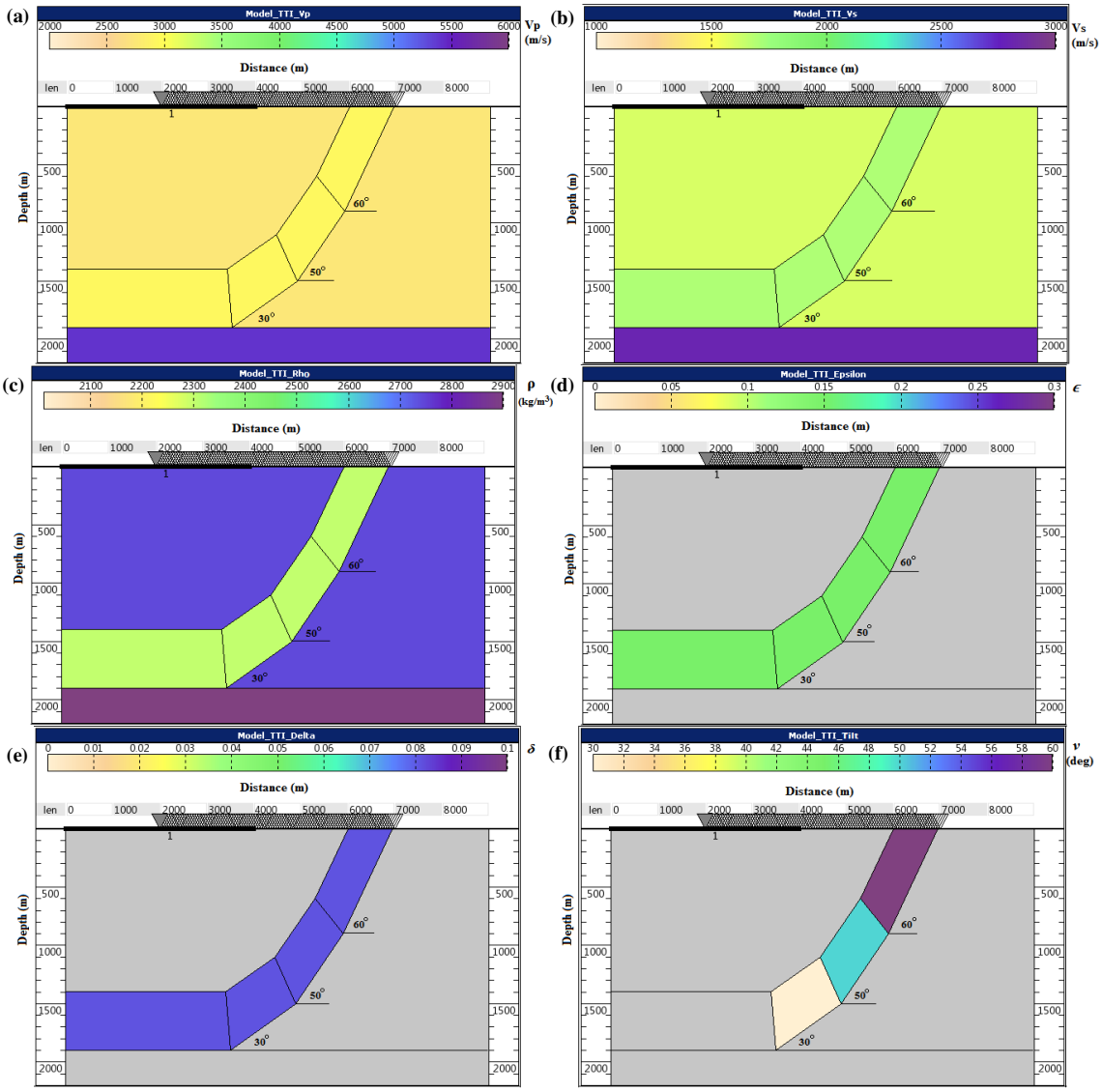

Figure 1: Tilted transversely isotropic (TTI) thrust sheet (a) with variable dips for different blocks $(0^{\circ}, 30^{\circ}, 50^{0}, 60^{\circ})$ and the corresponding symmetry axis are orthogonal to the sheets bottom. Except for the symmetry-axis direction, the parameters of all TTI blocks are the same. The TTI thrust sheet is embedded within the homogeneous and isotropic background having a flat base. The true model parameters used for elastic staggered-grid finite-difference full-wave seismic modeling are shown as (a) P-wave velocity (V_P), (b) S-wave velocity (V_S), (c) density (ρ), Thomsen's parameters in (d) for ϵ, (e) for δ and tilts of the TTI thrust sheet in (f) for ν. The receivers are shown as black squares and sources as inverted triangles on the top of the model. The color scale for each figure represents the corresponding values of the of the model parameters.

the physical model corresponding to the over-thrust areas such as Canadian Foothills, where the exploration targets often lie below the thrusted shale layer (Leslie and Lawton, 1998). The model resembling the TTI thrust belts of the Canadian Foot Hills chosen for seismic imaging is characterized by weak TI thrust sheet consists of four blocks with dips 0°, 30°, 50° and 60° from the vertical (Fig. 1), which

are embedded in a background medium that is elastic and isotropic (V_{P0}=2740 m/s, V_{S0}=1600 m/s, ρ=2740 kg/m^3). All four blocks are elastic, homogeneous and anisotropic (V_{P0}=2925 m/s, V_{S0}=1700 m/s, ρ=2300 kg/m^3, ϵ=0.15, δ=0.081, γ=0.035, and tilts $\nu = 0^\circ, 30^\circ, 50^\circ$ and 60°) with the TI symmetry axis for each block is orthogonal to the bedding within. The reflector below the TTI thrust sheet represents the horizontal target-layer of exploration interest (V_{P0}=5402 km/s, V_{S0}=2800 m/s, ρ=2900 kg/m^3). The dimension of the model is $9000\text{ m} \times 2200\text{ m}$ in the horizontal (x) and vertical (z) directions and the mesh is generated with 1 m grid spacing. There are many numerical modeling techniques available to model the TTI thrust sheet, but full-wave elastic anisotropic finite-difference modeling using the staggered grid scheme with fourth-order approximations is considered as very powerful and more accurate (Igel *et al*., 1995; Juhlin, 1995; Operto *et al*., 2009), which is used in this study. The absorbing boundary conditions also imposed to reduce the edge effects while modeling. Free-surface boundary condition at the top of the model is imposed to reduce the numerical phases or other spurious arrivals that contaminate the synthetic seismic data.

Methodology

Elastic constants

In elastic media, stresses and strains are related by generalized Hooke's law, which can be expressed as

$$\boldsymbol{\sigma}_{ij} = \boldsymbol{C}_{ijkl}\boldsymbol{\epsilon}_{kl}, \tag{1}$$

where $\boldsymbol{\sigma}$ is the stress tensor, $\boldsymbol{\epsilon}$ is the strain tensor, and $\boldsymbol{C}$ is the $3 \times 3 \times 3 \times 3$ tensor of elastic constants. In the 3-D case, subscript $i, j, k,$ and l can be taken as 1, 2, and 3. The symmetric components of the stress and strain tensor can be expressed as six independent components. Similarly, the tensor of elastic constants can be written as 6×6 matrix of elastic constants. In the 2-D case, in which strain is free in the *y*-axis, the matrix of elastic constants in a VTI medium that has a vertical symmetry-axis of anisotropy can be written as

$$C_{\alpha\beta} = \begin{pmatrix} C_{11} & C_{13} & 0 \\ C_{13} & C_{33} & 0 \\ 0 & 0 & C_{55} \end{pmatrix} \tag{2}$$

In this form, the *P*-wave velocities in the vertical $(\theta = 0^\circ)$ and horizontal $(\theta = 90^\circ)$ directions with respect to the symmetry axis are expressed as

$$V_{P0} = \sqrt{\frac{C_{33}}{\rho}},$$

$$V_{P90} = \sqrt{\frac{C_{11}}{\rho}},$$

and *SV*-wave velocity

$$V_{SV}(\theta = 90^\circ) = V_{SV}(\theta = 0^\circ) = \sqrt{\frac{C_{55}}{\rho}}$$

where ρ is the density of the material. This also indicates that vertical and horizontal *P*-wave velocities are generally different unless $C_{33} = C_{11}$ and equal to each other for the *SV*-wave. The velocity of *SV*-wave, however vary at oblique angle of incidence $(0^\circ < \theta < 90^\circ)$ and the only TI model with a constant V_{SV} is elliptical (Tsvankin, 2005). The three dimensionless anisotropic parameters denoted as ϵ, δ and γ can be expressed as

$$\epsilon = \frac{c_{11} - c_{33}}{\rho}, \delta = \frac{(c_{13} + c_{55})^2 - (c_{33} - c_{55})^2}{2c_{33}(c_{33} - c_{55})},$$
$$\gamma = \frac{c_{66} - c_{55}}{2c_{55}}, \tag{3}$$

In Thomsen notation, *P* and *SV*-wave signatures depend on the parameters V_{P0}, V_{S0}, ϵ and δ, while the *SH*-wave is fully described by the shear-wave vertical velocity V_{S0} and γ. The strength of anisotropy is characterized by these three dimensionless parameters ϵ, δ and γ for which ϵ defines *P*-wave anisotropy and γ represents *SH*-wave anisotropy. The parameter δ is a measure of second derivative of *P*-wave phase velocity function at vertical angle of incidence, which is responsible for the angular dependence of V_P in the vicinity of the vertical (symmetry direction), which increases away from the vertical if $\delta > 0$ and decreases if $\delta < 0$ (Tsvankin, 2005).

In a 2-D TTI medium having tilted axis of symmetry, the matrix of elastic constants has six independent components. Hence, the matrix of elastic constants can be rewritten as

$$\begin{pmatrix} C_{11} & C_{13} & C_{15} \\ C_{13} & C_{33} & C_{35} \\ C_{15} & C_{35} & C_{55} \end{pmatrix} \tag{4}$$

Each component of this matrix can be calculated from the matrix of VTI medium (eq. 2) by using the rotation tensor (Han *et al.*, 2012).

Equations of motion for 2-D media

The 2-D velocity-stress formulation for elastic wave propagation in an isotropic medium can be expressed in terms of elastodynamic wave equations as presented by Virieux (1986) and Levander (1988). In 2-D isotropic media, the elastodynamic wave equations can be written as

$$\begin{aligned}
\frac{\partial v_x}{\partial t} &= \frac{1}{\rho}\left(\frac{\partial \sigma_{xx}}{\partial x} + \frac{\partial \sigma_{xz}}{\partial z}\right),\\
\frac{\partial v_z}{\partial t} &= \frac{1}{\rho}\left(\frac{\partial \sigma_{xz}}{\partial x} + \frac{\partial \sigma_{zz}}{\partial z}\right),\\
\frac{\partial \sigma_{xx}}{\partial t} &= (\lambda + 2\mu)\frac{\partial v_x}{\partial x} + \lambda\frac{\partial v_z}{\partial z},\\
\frac{\partial \sigma_{zz}}{\partial t} &= (\lambda + 2\mu)\frac{\partial v_z}{\partial z} + \lambda\frac{\partial v_x}{\partial x},\\
\frac{\partial \sigma_{xz}}{\partial t} &= \mu\left(\frac{\partial v_x}{\partial z} + \frac{\partial v_z}{\partial x}\right),
\end{aligned} \tag{5}$$

where v_x and v_z are particle velocities, σ_{xx} , σ_{zz} and σ_{xz} are stress components, λ and μ are the Lamé coefficients. Lamé coefficients are related to elastic constants by $C_{11} = C_{33} = \lambda + 2\mu$ and $C_{55} = \mu$ for an isotropic medium. In the TTI medium, the equations have to be modified because the six components of elastic constants influence the wave motion. Thus, the 2-D velocity-stress formulation is given as

$$\begin{aligned}
\frac{\partial v_x}{\partial x} &= \frac{1}{\rho}\left(\frac{\partial \sigma_{xx}}{\partial x} + \frac{\partial \sigma_{xz}}{\partial z}\right),\\
\frac{\partial v_z}{\partial t} &= \frac{1}{\rho}\left(\frac{\partial \sigma_{xz}}{\partial x} + \frac{\partial \sigma_{zz}}{\partial z}\right),\\
\frac{\partial \sigma_{xx}}{\partial t} &= C_{11}\frac{\partial v_x}{\partial x} + C_{13}\frac{\partial v_z}{\partial z} + C_{15}\left(\frac{\partial v_x}{\partial z} + \frac{\partial v_z}{\partial x}\right),\\
\frac{\partial \sigma_{zz}}{\partial t} &= C_{13}\frac{\partial v_x}{\partial x} + C_{33}\frac{\partial v_z}{\partial z} + C_{35}\left(\frac{\partial v_x}{\partial z} + \frac{\partial v_z}{\partial x}\right),\\
\frac{\partial \sigma_{xz}}{\partial t} &= C_{15}\frac{\partial v_x}{\partial x} + C_{35}\frac{\partial v_z}{\partial z}\\
&\quad + C_{55}\left(\frac{\partial v_x}{\partial z} + \frac{\partial v_z}{\partial x}\right).
\end{aligned} \tag{6}$$

2-D staggered grid scheme

On a staggered grid, variables such as velocity and stress are defined not only at grid points but also at half-grid points, while on a regular grid all the material properties are defined at the same grid points (Virieux, 1986; Graves, 1996). Thus, the velocity and stress components are set to different spatial positions as shown in Fig. 2. Such a scheme is very efficient, which converges faster and results in improved accuracy.

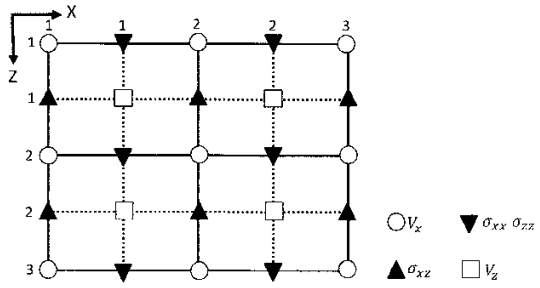

Figure 2: Spatial locations of velocity (V_x, V_z) and stress components ($\sigma_{xx}, \sigma_{zz}, \sigma_{xz}$) on a finite difference staggered grid.

In order to realize the free surface boundary condition, normal stress (σ_{zz}) and shear stress (σ_{xz}) should be set to zero at the boundary grids. However, on a staggered grid, shear stress is defined at a half-grid point, whereas normal stress is defined at a grid point (Fig. 2). Thus, normal stress can easily satisfy the free surface boundary condition to substitute a zero value, because it is defined at a grid point. On the other hand, shear stress at the auxiliary two rows should have the same value but opposite sign based on the free surface. Therefore, to meet the free surface boundary condition for shear stress on a staggered grid scheme, auxiliary grid points are needed in the z-direction.

Boundary conditions and validation of staggered grid scheme

To validate the performance of the staggered grid scheme for wave propagation (snapshots) and generation of full-wave synthetic seismic data (shot gathers) for the TTI thrust sheet (Fig. 1) used for elastic anisotropic finite-difference modeling, the model was first discretized both in horizontal and vertical directions with grid sizes (Δx and Δz) of 1 m. The Ricker wavelet with 25 Hz as main frequency and time step (Δt) used in the explicit time integration scheme chosen as 0.2 ms which satisfies the stability criteria of the fourth-order approximation proposed by Levander (1998):

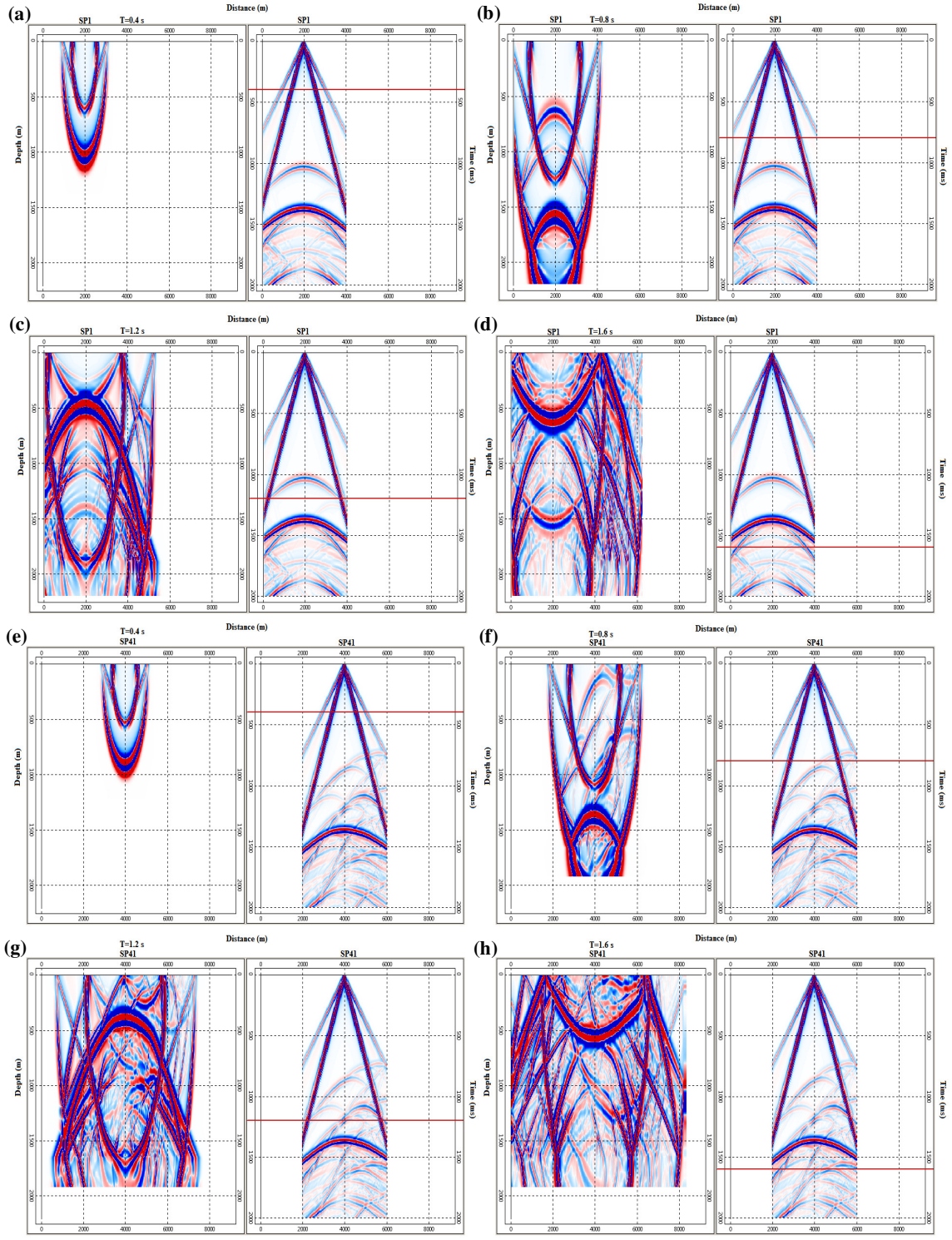
(a)
SP1
T=0.4 s
SP1
Distance (m)
Depth (m)
Time (ms)
(b)
SP1
T=0.8 s
SP1
Distance (m)
Depth (m)
Time (ms)
(c)
SP1
T=1.2 s
SP1
Distance (m)
Depth (m)
Time (ms)
(d)
SP1
T=1.6 s
SP1
Distance (m)
Depth (m)
Time (ms)
(e)
T=0.4 s
SP41
SP41
Distance (m)
Depth (m)
Time (ms)
(f)
T=0.8 s
SP41
SP41
Distance (m)
Depth (m)
Time (ms)
(g)
T=1.2 s
SP41
SP41
Distance (m)
Depth (m)
Time (ms)
(h)
T=1.6 s
SP41
SP41
Distance (m)
Depth (m)
Time (ms)

Figure 3: The snapshots of wave propagation at different times (a) T=0.4 s, (b) T=0.8 s, (c) T=1.2 s, (d) T=1.6 s for shot point SP1 at 2000 m and at times (e) T=0.4 s (f) T=0.8 s (g) T=1.2 s, and (h) T=1.6 s for SP41 at 4000m of the model distance shown in the left panel. The corresponding generated full-wave synthetic seismic data for the same SP's are shown in the right panel against each snapshot with a red rubber line indicating the exact time of wave propagation through the model.

$$\Delta t < 0.606 \frac{\Delta x (= \Delta z)}{v_{p,max}}, \quad (7)$$

Absorbing boundary conditions with ten grid points added to the left, right and bottom boundaries to absorb artificial reflections. Free surface condition was applied to the top boundary for elastic wave propagation (Fig. 3) and computation of full-wave synthetic seismic data (Fig. 3) for the TTI thrust sheet (Fig. 1).

Synthetic Seismic Data

Based on these model parameters (Fig. 1) and employing a robust staggered-grid computing scheme for elastic anisotropic finite-difference full-wave modeling, the synthetic 2-D seismic data generated shows very good quality (Fig. 3) with distinct phases which are very clear for each shot gathers generated. The data consists of 101 shot gathers (SP1 to SP101) spanning from 2000 m to 7000 m horizontally for this model (Fig. 1) with shot interval of 50 m and number of receivers for each shot is 161 with receiver interval of 25 m. The data acquisition is made with symmetric split-spread configuration with maximum offset from each shot is ±2000 m. The record length (two-way time) of the data is 2 s with 2 ms SI (sample interval) and zero-phase Ricker-wavelet of dominant frequency 25 Hz is used as a source wavelet. The nature of wave propagation (snapshots) at different time steps through the model and the corresponding example shot gather generated for this are shown in Fig 3. The seismic data has been acquired by moving the whole receiver spread for each shot similar to simulate a real field recording along a 2-D seismic line over the TTI thrust model (Fig. 1) using common depth point (CDP) technique.

Elastic wave propagation for the TTI model

The snapshots of wave propagation at different time steps of 0.4 s intervals after shooting is illustrated in Fig. 3 for a typical shot points SP1 at 2000 m and SP41 at 4000 m distance of the TTI model. The corresponding synthetic seismic data generated by elastic anisotropic wave propagation through the model are shown for the respective SP's in which the time of wave propagation represented by a red rubber line. In the snapshots of the wave propagation and the corresponding synthetic seismic data (Fig. 3) the *P*-wave, *S*-wave, Rayleigh wave (ground roll), and *P*-*SV* mode conversions, reflections from the different interface boundaries, multiples and generation of all type of phases for all the shots of the TTI thrust model are prominent because a robust elastic anisotropic finite-difference full-wave modeling using staggered grid scheme is adopted.

Anisotropic MVA and Depth Imaging

The synthetic seismic data generated (Fig. 3) are used for Kirchhoff pre-stack depth migration using migration velocity analysis (MVA) technique (Behera and Tsvankin, 2009) for imaging the TTI Thrust sheet. Fourth-order approximations have been used for traveltime computations using an anisotropic ray-tracer, which could able trace rays down to the bottom of the thrust for each source and receivers. These traveltimes computed for the model are used for the anisotropic Kirchhoff depth migration followed by MVA iteratively to obtain improvements of the image taking into consideration the symmetry direction velocity V_{P0}, Thomsen's parameters ϵ, δ and tilt of each blocks ν of the TTI Thrust sheet. The final depth migrated image is obtained after six iterations MVA and update of model parameters in each iteration. The final model parameters obtained are very close to the true parameters and the true model is shown in the background of the final depth migrated image obtained (Fig. 4) showing very good correlation with the model except below 6000 m of profile distance, which indicates the tilt is significantly high for the Kirchhoff anisotropic depth migration. The target layer below the thrust sheet has been well imaged without much distortion, which indicates the imaging algorithm employed is stable to handle tilts close to 60°, which are a common problem of the overthrust regions of the Canadian Foothills or highly dipping beds in the Foothills of the Himalaya.

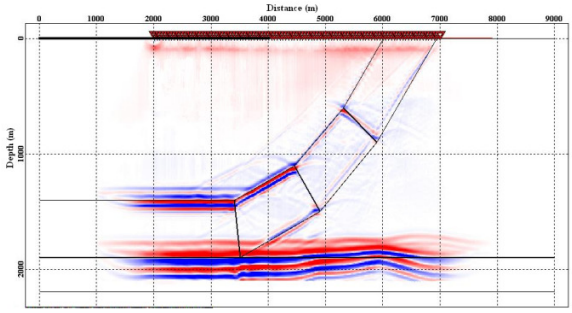

Figure 4: Final depth image obtained using anisotropic Kirchhoff pre-stack depth migration and migration velocity analysis (MVA) to update the model parameters. The source locations are shown as inverted triangles used for generation the synthetic shot gathers used in this study.

Conclusions

The present study provides an important insight about the generation of full-wave synthetic seismic data to simulate the actual field conditions and image sub-surface structures in a very complex geological setting in the Foothills of Canada and Himalaya, where the dipping beds are over thrusted representing a TTI model. The tilts of the beds are very high ($> 60^{\circ}$), which poses severe imaging problems of target zones for hydrocarbon plays lying below the steeply dipping TTI layers due to poor focusing and mispositioning of events because of severe contamination of different types of noises like scattering, diffractions, multiples, converted waves, which are responsible for poor imaging of reflections.

Acknowledgments

I thank the Director, CSIR-NGRI for according permission to publish the paper. The elastic staggered-grid numerical computations are performed using massively parallel codes of Tesseral. Funding from PSC0205 (LB) SHORE (CSIR) and GAP-523-28 (LB) of SERC-DST are duly acknowledged.

References

Behera, L. and Tsvankin, I., 2009, Migration velocity analysis for tilted transversely isotropic media; Geophysical Prospecting, 57, 13-26.

Graves, R. W., 1996, Simulating seismic wave propagation in 3D elastic media using staggered-grid finite differences; Bulletin of Seismological Society of America, 86, 1091-1106.

Grechka, V., Pech., A., Tsvankin, I. and Han, B., 2001, Velocity analysis for tilted transversely isotropic media: A physical modeling example; Geophysics, 66, 904-910.

Han., B., Seol, S. J. and Byun, J., 2012, Elastic modeling in tilted transversely isotropic media with convolutional perfectly matched boundary conditions; Exploration Geophysics, 43,77-86.

Igel, H., Mora, P. and Riollet, B., 1995, Anisotropic wave propagation through finite-difference grid; Geophysics, 60, 1203-1216.

Isaac, J. H. and Lawton, D. C., 1999, Image mispositioning due to dipping TI media: A physical seismic modeling study; Geophysics, 64, 1230-1238.

Juhlin, C., 1995, Finite-difference elastic wave propagation in 2D heterogeneous transversely isotropic media; Geophysical Prospecting, 43, 843-858.

Kumar, C., Sen, M. K. and Fergusen, R. J., 2008, Depth migration anisotropy analysis in the time domain; Geophysical Prospecting, 56, 87-94.

Leslie, J. M. and Lawton, D. C., 1998, A refraction seismic field study to determine the anisotropic parameters of shales; The Leading Edge, 17, 1127-1129.

Levander, A. R., 1988. Fourth-order finite-difference P-SV seismograms; Geophysics, 53, 1425-1436.

Operto, S., Virieux, J., Ribodetti, A. and Anderson, J. E., 2009, Finite-difference frequency-domain modeling of viscoacoustic wave propagation in 2D tilted transversely isotropic (TTI) media; Geophysics, 74, T75-T95.

Thomsen, L., 1986, Weak elastic anisotropy; Geophysics, 51, 1954-1966.

Tsvankin, I., 2005, Seismic signatures and analysis of reflection data in anisotropic media, 2nd edition; Elsevier Science Publishing Co.

Vestrum, R., Lawton, D. C. and Schmid, R., 1999, Imaging structures below dipping TI media; Geophysics, 64, 1239-1246.

Virieux, J., 1986, P-SV wave propagation in heterogeneous media: velocity-stress finite-difference method; Geophysics, 51, 889-901.